# Adsorption of Pb (II) Ions onto Hydroxyapatite Nanopowders in Aqueous Solutions

Simona Liliana Iconaru, Mikael Motelica-Heino, Régis Guégan, Mircea Beuran, Adrian Costescu, Daniela Predoi

materials

MDPI

Article

# Adsorption of Pb (II) Ions onto Hydroxyapatite Nanopowders in Aqueous Solutions

**Simona Liliana Iconaru [1], Mikael Motelica-Heino [2], Regis Guegan [3], Mircea Beuran [4,5], Adrian Costescu [6] and Daniela Predoi [1,*]**

1 National Institute of Materials Physics, Atomistilor Street, No. 405A, P.O. Box MG 07, 077125 Magurele, Romania; simonaiconaru@gmail.com
2 ISTO, UMR 7327 CNRS Université d'Orléans, 1A rue de la Férollerie, 45071 Orléans CEDEX 2, France; mikael.motelica@univ-orleans.fr
3 Faculty of Science and Engineering, Global Center for Science and Engineering, Waseda University, 3-4-1, Okubo, Shinjuku-ku, Tokyo 169-8555, Japan; regis.guegan@aoni.waseda.jp
4 Carol Davila University of Medicine and Pharmacy, 8 Eroii Sanitari, Sector 5, 050474 Bucharest, Romania; beuranmircea@gmail.com
5 Emergency Hospital Floreasca Bucharest, 8 Calea Floresca, 014461 Bucharest, Romania
6 Faculty of Exact Sciences & Engineering, Hyperion University of Bucharest, 169 Calea Călărași, 030615 Bucharest, Romania; adrian.costescu@gmail.com
* Correspondence: dpredoi@gmail.com; Tel.: +40-723751972

Received: 30 September 2018; Accepted: 5 November 2018; Published: 7 November 2018


**Abstract:** Contamination of water with heavy metals such as lead is a major worldwide problem because they affect the physiological functions of living organisms, cause cancer, and damage the immune system. Hydroxyapatite, ($Ca_5(PO_4)_3OH$) is considered one of the most effective materials for removing heavy metals from contaminated water. The hydroxyapatite nanopowders (N-HAp) obtained by a co-precipitation method were used in this research to determine the effectiveness in removing lead ions from contaminated solutions. In this study, we have investigated the structure and morphology of N-HAp nanopowders using X-ray diffraction (XRD), electronic transmission microscopy (TEM), and scanning electron microscopy (SEM). The structure information was also obtained by spectroscopy measurements. The Fourier transform infrared spectroscopy (FTIR) and Raman spectroscopy measurements revealed the presence of peaks corresponding to the phosphate and hydroxyl groups. The ability of N-HAp nanopowders to adsorb lead ions from aqueous solutions were established. The results of the kinetic and equilibrium studies on the removal of Pb (II) from aqueous solution revealed that the adsorption of lead (II) cations is due to the surface reaction with the hydroxyl terminal groups on the adsorbent and the combination of the positive charges of the metal cations with the negative charges on the adsorbent surfaces. These observations could validate the use of these ceramic nanopowders in ecological remediation strategies.

**Keywords:** hydroxyapatite nanoparticles; lead; water depollution

## 1. Introduction

The economic development and rapid industrialization from recent years created many hazardous waste areas that contribute to the widespread contamination of soil and groundwater all over the world. These include often-abandoned mining sites, landfills, industrial areas, oil reservoirs, etc. The continued expansion of contaminated areas is a major environmental problem in the modern world. In this context, researchers around the world have turned their attention to finding efficient and cost-effective new methods of depollution, bearing in mind, that majority of pollutants such as heavy metals are not biodegradable and tend to accumulate in living organisms, inflicting serious

damage to various vital functions and serious illnesses [1–4]. The conventional techniques studied so far and currently used in the environment rehabilitation have many disadvantages. Methods such as treating or aerating the soil, removing soil vapors or burning industrial residues used up until now have been reported to be expensive and to have a harmful impact on the ecosystem [5–7]. Because of these inconveniences, it is envisaged to develop technologies that will enable the environment to be rehabilitated using eco-friendly and cost-effective technologies. For the purpose of streamlining techniques for treating and preserving the environment, particular attention has been given to nanomaterials with biocompatible properties [8–12]. Numerous laboratory studies have been carried out in recent years on various materials with potential applications for the conservation and treatment of the environment. Among the studied materials, special attention was granted to hydroxyapatite-based composites for the purpose of decontamination of soils, ocean and/or continental waters. Even though they are well known for applications in the biomedical field, apatites possess a strong affinity for heavy metal sorption [10–16]. Currently, many studies have been focused on the development of apatites with mesoporous structure and high specific surface area, which gives them a high capacity to adsorb heavy metals from contaminated waters and soils. Existing literature studies involving the adsorption properties of porous and poorly crystalline apatites are very rare. Interaction of apatites with both metals and radionuclides is an ongoing research topic. The adsorption mechanisms presented by various laboratory investigations vary depending on the adsorbed cation. Suzuki and co-workers, [17] in their studies on the mechanism of adsorption of ions such as $Pb^{2+}$, $Cu^{2+}$, $Cd^{2+}$, $Zn^{2+}$, $Ni^{2+}$, $Co^{2+}$, $Mn^{2+}$, $Mg^{2+}$, and $Ba^{2+}$ explained their adsorption by apatite as the result of an ion exchange. During the years, numerous models have been developed to obtain a detailed description of the metallic ions adsorption onto different kind of materials [18–20]. F. Di Natale et al. [19] in their studies describe a model for metallic ions adsorption from aqueous solutions using activated carbons, while Erto et al. [20] in their paper regarding the adsorption of cadmium and zinc onto activated carbon, emphasize that the most adequate model to predict adsorption data in the case of cadmium and zinc adsorption on activated carbon is by using the Extended Langmuir model. Moreover, their results showed that in the case of cadmium adsorption better results were obtained using the Vacancy Solution Theory (VST).

Middelburg and Comans [21] in their studies on the use of hydroxyapatite for $Cd^{2+}$ sorption described the heavy metal transport model in hydroxyapatite through sorption reactions and transport physical processes. The immobilization of lead from aqueous solutions with hydroxyapatite has been also described by Xu and Schwartz [22] as being achievable as a result of the dissolution/precipitation mechanisms occurring during the adsorption process. The data obtained by now has concluded that the use of nanoparticle-based nanostructured materials [23,24] can lead to the development of far more efficient technologies for decontamination of soils and waters at much lower costs compared to techniques based on micro- and/or macroscopic materials. Due to its high porosity and affinity to heavy metal ions, apatite and calcium phosphate materials are considered some of the most promising materials to obtain effective environmental technologies.

The aim of this study was to obtain hydroxyapatite nanoparticles with a high affinity for heavy metal ions. The physico-chemical properties of hydroxyapatite nanopowders N-HAp, obtained by coprecipitation have been investigated using XRD, TEM, SEM, FTIR, and Raman. The affinity towards lead ions of the N-HAp nanopowders has been studied by batch adsorption experiments.

## 2. Materials and Methods

### *2.1. Synthesis of Hydroxyapatite Nanoparticles (HAp)*

The hydroxyapatite, nanoparticles, $Ca_{10}(PO_4)_6(OH)_2$, were obtained using an adapted coprecipitation method which was previously detailed in [25,26].

The reagents for synthesis, calcium nitrate [$Ca(NO_3)_2 \cdot 4H_2O$] and ammonium dihydrogen phosphate [$(NH_4)_2HPO_4$] were purchased from Alpha Aesare, Karlsruhe, Germany. The $Ca_{10}(PO_4)_6(OH)_2$, with

x = 0 (HAp), nano powder was synthesized by an adapted co-precipitation method (Ca/P molar ratio: 1.67) using [$(NH_4)_2HPO_4$] and $Ca(NO_3)_2{\cdot}4H_2O$ [27]. The hydroxyapatite nanoparticles was effectuated by adjustment the atomic ratio Ca/P as 1.67. A designed amount of $Ca(NO_3)_2{\cdot}4H_2O$ were dissolved in deionised water to obtain 400 mL Ca-containing solution. In the same time, a designed amount of ammonium dihydrogen phosphate $(NH_4)_2HPO_4$ was dissolved in deionised water to make 400 mL P-containing solution. The two solutions were agitated at 100 °C during 40 min. The P-containing solution was added drop by drop into the Ca-containing solution. The pH of resulting mixture was kept constant during the reaction by adding $NH_3$ and stirred continuously for 4 h. The resulting final mixture was filtered and washed several times with deionized water. Finally, the recovered powder was dried in an oven at 100 °C for 72 h. The resulting powder after drying was used in the experiments in this study.

### *2.2. Structural and Morphological Characterizations*

The structure and morphology of the hydroxyapatite nanoparticles obtained by coprecipitation were characterized by XRD, SEM, EDX and TEM. Investigations of XRD were performed for the N-HAp nanopowders with a Bruker D8 Advance diffractometer (Bruker, Karlsruhe, Germany) having a nickel filtered Cu K$\alpha$ ($\lambda$ = 1.5418 Å) radiation and a high efficiency one-dimensional detector (Lynx Eye type, Bruker, Karlsruhe, Germany) operated in integration mode. The measurements were recorded over the 2$\theta$ range of 20–80°, using a step size of 0.02° and 34 s measuring time per step. The morphology and the elemental composition of the N-HAp nanopowders was investigated by scanning electron microscopy (SEM) using a HITACHI S4500 microscope (Tokyo, Japan) equipped with an X-ray Energy Dispersive Spectroscopy (EDX) system.

Furthermore, the size and morphology of the N-HAp nanopowders were analyzed using transmission electron microscopy (TEM) with a CM 20 (Philips—FEI, Eindhoven, Netherlands), equipped with a filament Lab6 that works at 200 kV. For TEM observation, the N-HAp nanopowders were dispersed in ethanol using an ultrasonic bath (Retsch GmbH, Haan, Germany) and a drop of the resulting solution was deposited on a carbon-coated Cu grid and left to dry for 24 h at room temperature before visualization. Information about the specific surface area, pore volume, pore size and particle size of the samples was obtained by adsorption-desorption (nitrogen, $N_2$) gas analysis using Brunauer–Emmett–Teller (BET) method using an ASAP 2020 (Micromeritics Instrument Corp, Norcross, GA, USA) instrument.

### *2.3. Batch Adsorption Experiments*

The efficiency of lead adsorption onto hydroxyapatite nanopowders was investigated by batch adsorption experiments. The batch adsorption experiments were performed using silicon tubes with aqueous solutions containing lead ions in a concentration range of 0–100 mg $L^{-1}$. The contaminated lead solution were obtained using $Pb(NO_3)_2$ (Alpha Aesar, Alfa Aesar, Karlsruhe, Germany; 99% purity) and distilled water. The amount of the N-HAp nanopowders used, as adsorbent was 0.2 g and the solution pH of the initial contaminated solution was adjusted to a value of 5 $\pm$ 0.4 using a 0.1 M hydrochloric acid (HCl) solution. During the batch adsorption experiments, the solution volume was kept at 20 mL and the mixture was stirred on a Mixer SRT1 Roller (Stuart Scientific, Staffordshire, UK) for 48 h. After 48 h, the tubes were centrifuged for 1 h at 10,000 rpm. The supernatant was filtered, recovered and analyzed by Flame Atomic Absorption Spectrometry (AAS) using a Zeeman HITACHI Z-8100 from Japan Hitachi (Tokyo, Japan). The AAS measurements were conducted under a constant air flow rate at a wavelength of 283.3 nm according to the operational condition for lead. The batch experiments were carried out at room temperature, in triplicate.

## 3. Results and Discussions

The structure, morphology and elemental analysis were presented in Figure 1. In order to highlight the crystalline structure of the obtained hydroxyapatite samples, XRD measurements were performed. Furthermore, in order to obtain conclusive results, N-HAp nanopowders were also analyzed by TEM. For the morphological characterization and determination of the elemental composition of the N-HAp samples, an electronic scanning microscope equipped with an EDX system was used. Figure 1a shows the diffraction patterns of N-HAp nanoparticles obtained by co-precipitation. The TEM image for the N-HAp powders are presented in Figure 1b. SEM micrographs and EDX spectra for N-HAp powders are also shown in Figure 1c,d, respectively.

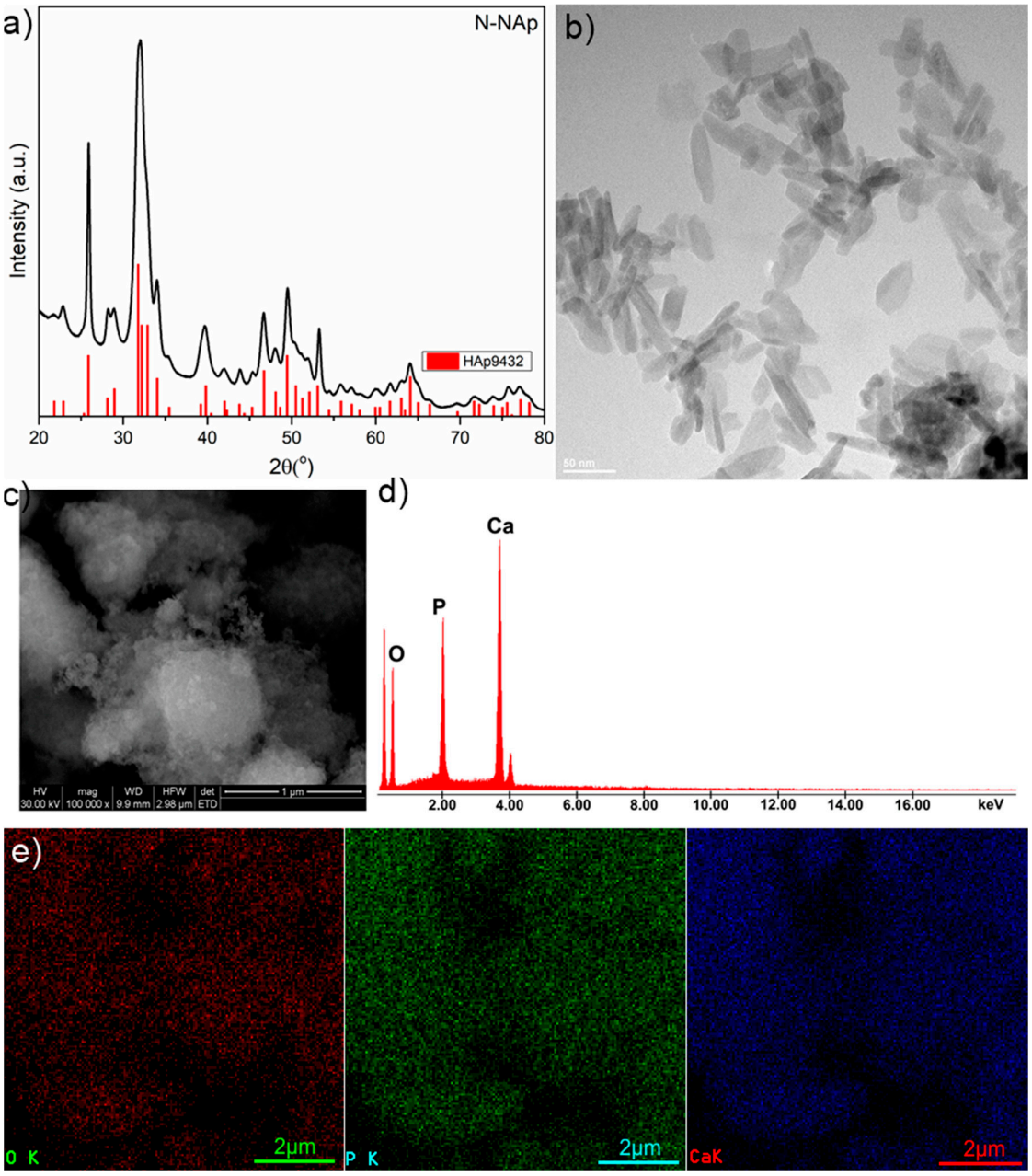


**Figure 1.** XRD patterns of hydroxyapatite nanopowders (N-HAp) nanopowders and ICDD-PDF (International Center for Diffraction Data- Powder Diffraction File) 9-432 (**a**); TEM image of N-HAp nanopowders (**b**); SEM micrograph of N-HAp (**c**); EDX spectra of N-HAp nanopowders (**d**); elemental mapping of N-HAp nanopowders (**e**).

As it can be seen from Figure 1a, the peaks occurring in the diffraction patterns of N-HAp are characteristic to hexagonal hydroxyapatite in agreement with the ICDD-PDF (International Center for Diffraction Data- Powder Diffraction File) 9-432, indicating that the analyzed powders exhibit a characteristic HAp hexagonal structure [28–32]. Moreover, the diffraction patterns characteristic to the theoretical diffraction patterns of the hexagonal hydroxyapatite (ICDD-PDF 9-432) are also shown in Figure 1a (in red). Furthermore, no additional peaks were found in the diffraction pattern of N-HAp. The TEM image (Figure 1b) revealed that the hydroxyapatite particles obtained by co-precipitation are of nanometric dimensions and ellipsoidal shape. The SEM analysis of the N-HAp particles revealed that they have nanometric size and ellipsoidal shape in accordance with the information obtained from TEM images (Figure 1c). From the EDX spectrum (Figure 1d), it can be observed that only the constitutive elements of hydroxyapatite (calcium (Ca), phosphorus (P), and oxygen (O)) have been highlighted in the analyzed sample. The elemental mapping of N-HAp nanopowders (Figure 1e) demonstrated that the constituent elements were evenly distributed in the samples.

FTIR was used for the determination of the functional groups of N-HAp nanopowders [27,33–35]. The analyzed N-HAp FTIR spectrum was performed in the range of 400–2000 $cm^{-1}$ with a resolution of 4 $cm^{-1}$ and 256 scans (Figure 2a). In order to obtain complementary information, the N-HAp powders were also investigated using Raman spectroscopy (Figure 2b). The Raman spectrum was carried out in the range of 400–1200 $cm^{-1}$. Figure 2a presents the FTIR spectra of N-HAp nanopowders obtained in transmission mode. The spectrum reveals the presence of the vibrational modes corresponding to phosphate and hydroxyl groups. The main vibrational bands characteristic to phosphate groups were observed at 474 $cm^{-1}$, 571 $cm^{-1}$, and 604 $cm^{-1}$. The clear presence of these three bands confirms the formation of hydroxyapatite. The vibration band corresponding to the $HPO_4^{2-}$ group was also observed at 876 $cm^{-1}$. The vibrational bands corresponding to the surface adsorbed water were highlighted in the 1600–1700 $cm^{-1}$ interval. The Raman spectrum recorded for the N-HAp powders are shown in Figure 2b. It can be observed that the vibration bands characteristic to $PO_4^{3-}$ are present in the N-HAp sample spectrum in accordance with previous studies [34,35]. In the Raman spectrum, the band at 960 $cm^{-1}$, associated with the internal vibration modes of $\nu_1$ ($PO_4^{3-}$), (symmetrical stretching of the links P–O) can be clearly observed. The vibrational bands observed at 1026 $cm^{-1}$, 1049 $cm^{-1}$ and 1073 $cm^{-1}$ could be attributed to the elongation of the asymmetric link PO ($\nu_3$) while the vibrational bands from 576 $cm^{-1}$ or 590 $cm^{-1}$ and 616 $cm^{-1}$ are due to the vibration modes ($\nu_4$) of the phosphate group. The bands observed at 434 $cm^{-1}$ ($\nu_2$) and 431 $cm^{-1}$ ($\nu_2$) are assigned to O–P–O [34,35] bonds.

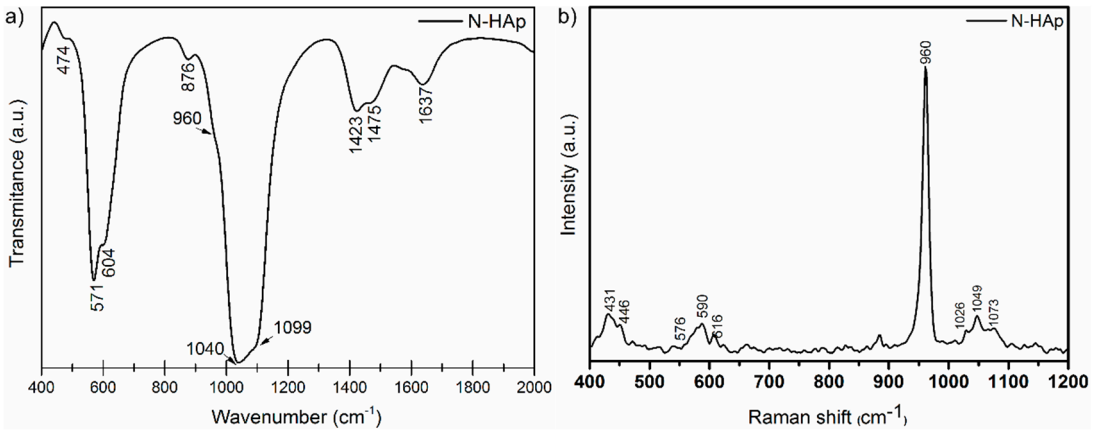


**Figure 2.** FTIR (**a**) and Raman (**b**) spectra of N-HAp nanopowders.

In order to obtain information regarding the specific surface area, pore volume, pore size, and particle size, gas adsorption/desorption studies have been carried out. The specific surface area (71.97 $m^2/g$) of the N-HAp powders was calculated using the BET (Brunauer, Emmet, Teller) method [36]. Moreover, the Barrett–Joyner–Halenda (BJH) analysis results for N-Hap samples were shown in Table 1.

The BET method [36] used to determine the specific surface of the samples is based on a proposed Brunauer, Emmett, and Teller theory and assumes that the surface is homogeneous and the adsorption is carried out in several layers, the molecules of the first layer serve as an adsorption site for the second layer. Moreover, during this process it is assumed that there is a permanent balance between the number of molecules adsorbed to the surface and those that are desorbed. Often, the BET equation is applicable only to a certain relative pressure range (between 0.05 and 0.1), region in which the theoretical and experimental curves coincide, as the BET theory does not take into account the heterogeneity of the solid material. On the other hand, the Barret–Joyner–Halenda (BJH) [37] model used is based on the condensation of nitrogen in mesopores that occurs at a pressure lower than the saturation vapor pressure of the absorbent. More of that, the BJH model uses the classical Kelvin law derived from the Laplace equation. Furthermore, it is well known that there is no unique definition of "pore diameter" or "pore size". Each method of determining the pore size defines a pore size in terms of a pore model that is most appropriate for the quantity measured in the experiment. In this study, flame atomic absorption spectroscopy measurements were used to measure lead ion concentration in order to assess the efficiency of the N-HAp powders in the removal of lead ions from aqueous solutions.

**Table 1.** Barrett-Joyner-Halenda (BJH) analysis results for N-Hap samples.

| N-HAp Information from BJH Analysis | | N-HAp |
|---|---|---|
| Cumulative pore surface area (Adsorption) obtained by the BJH method ($m^2/g$) | | 91.3 |
| Cumulative pore surface area (Desorption) obtained by the BJH method ($m^2/g$) | | 100.1 |
| Pore volume | Total pore volume (Absorption) ($cm^3/g$) | 0.025 |
| | Total pore volume (Desorption) ($cm^3/g$) | 0.4 |
| Pore size | Average pore size (Absorption) (nm) | 13.6 |
| | Average pore size (Desorption) (nm) | 22.6 |
| | The average pore diameter (Absorption) obtained by the BJH method (nm) | 18.23 |
| | The average pore diameter (Desorption) obtained by the BJH method (nm) | 16.66 |
| Particle size (nm) | | 83.37 |

For that purpose, the hydroxyapatite nanoparticles (N-HAp) were mixed with solutions having different concentrations of $Pb^{2+}$ (0–100 $mg \cdot L^{-1}$) and a pH value of 5. Figure 3 shows the efficiency of N-HAp nanopowders in the removal of lead ions from aqueous solutions. It can be seen that the lead removal efficiency depends on the initial concentration of $Pb^{2+}$. For a lead concentration of 20 mg $L^{-1}$, the removal efficiency of lead ions from the contaminated solution of N-HAp powders was 94%, thus demonstrating that the removal efficiency are dependent on the amount of the adsorbent, and on the initial $Pb^{2+}$ concentration.

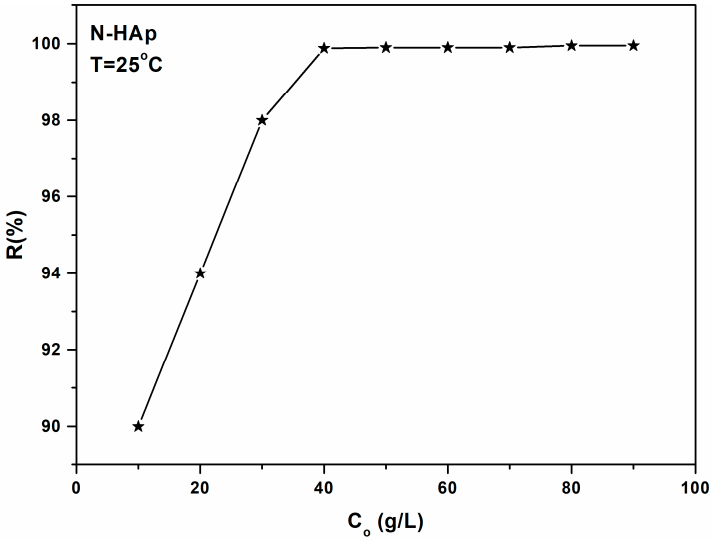


**Figure 3.** The effect of the initial concentration of $Pb^{2+}$ on the N-HAp efficiency in the removal of lead ions from aqueous solutions.

For lead concentrations in the range of 40–100 $mg \cdot L^{-1}$, it could be seen that the removal efficiency of $Pb^{2+}$ ions was about 99.2%. The removal efficiency of lead ions onto N-HAp nanopowders was calculated using the following formula:

$$R(\%) = \frac{(C_o - C_e)}{C_0} \times 100 \quad (1)$$

where $C_o$ and $C_e$ are the initial and equilibrium concentrations of $Pb^{2+}$ (g/L) ions.

For a complex understanding of the adsorption process, the effect of the pH of the initial lead solution was considered and batch experiments at four different pH values were undertaken. The results of the batch adsorption experiments for an initial concentration of $Pb^{2+}$ of 50 (g/L) are presented in Figure 4. This investigation has revealed that the pH value of the initial contaminated solution had an influence on the lead adsorption process onto N-HAp. According to the results, a removal efficiency of 99.2% was achieved for pH 5. On the other hand, the removal efficiency of lead ions by N-HAp powders was 96.7% at pH 4. For pH 3 and 2 the achieved removal efficiency was 95.3% and 93.8%. These results have emphasized that even though the efficiency of $Pb^{2+}$ ions from aqueous solution was influenced by the pH of the initial solution, at all the tested pH values, the removal efficiency was greater than 93%. Similar results regarding the influence of the pH value of the initial solution on the adsorption of lead from aqueous solutions were obtained by Cozmuta et al. [38]. Cozmuta et al. reported in their study that the decrease of pH induced a decrease of the maximum adsorption capacity of lead ions onto Na-clinoptilolite. The effect of the pH on the lead adsorption was also reported by Zhang et al. [39] in their studies regarding the "effect of temperature, salinity, and pH on the adsorption of lead by sediment of a tidal river in east China". The results presented by Zhang et al. emphasized an increase of Pb adsorption on sediment with the increase of pH values from 1 to 4. These results confirm that lead adsorption is strongly influenced by the initial pH value of the contaminated solution.

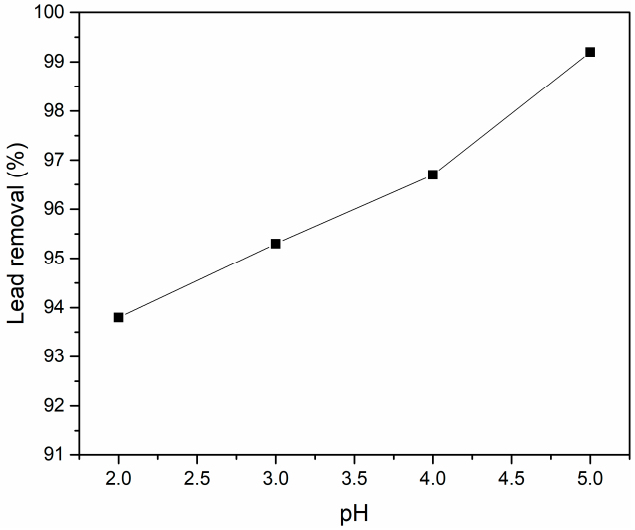


**Figure 4.** Effect of the solution pH on the removal of $Pb^{2+}$ ions by N-HAp powders.

In order to better understand and describe the processes of adsorption of metal ions on different materials, over the years, a wide range of models have been developed and employed: Langmuir; Freundlich; Brunauer–Emmett–Teller; Redlich–Peterson; Dubinin–Radushkevich; Temkin; Toth; Koble–Corrigan; Sips; Khan; Hill; Flory–Huggins; and Radke–Prausnitz [40]. The kinetic aspect plays an important role in all the models listed above. Thus, the adsorption equilibrium is defined as a dynamic equilibrium state, with both adsorption and desorption rates [41]. The physico-chemical parameters taken together with basic thermodynamic assumptions can provide an understanding of the adsorption mechanisms, surface properties, and adsorbent affinity [42]. To describe the adsorption process of lead ions on N-HAp powders, the Langmuir and Freundlich adsorption models were used [43].

In this study, the adsorption isotherms were obtained by mixing solutions containing different concentrations of $Pb^{2+}$ with a known amount of N-HAp powders until thermodynamic equilibrium at ambient temperature (T = 25 °C) was achieved. The adsorption capacity, defined as the amount of metal retained per mass unit, was estimated. Also, the quantity of $Pb^{2+}$ ions adsorbed at equilibrium per unit mass, $Q_e$, was determined using the formula:

$$Q_e = \frac{(C_0 - C_e)}{m} \quad (2)$$

where $C_o$ (mg/L) is the initial metal ion concentration, $C_e$ (mg/L) is the equilibrium concentration of Pb (II), V (L) is the volume of the solution, and m (g) is the mass of the adsorbent.

The Langmuir adsorption isotherm was originally developed to describe the gas-solid adsorption phase in activated carbon, and is most often used to quantify and emphasize the efficiency of a variety of biosorbents [41]. The empirical model involves the monolayer adsorption (the adsorbed layer has the thickness of a molecule). Adsorption can take place at a finite number of localized and defined areas that are identical and equivalent [44,45]. From a graphical point of view, the Langmuir isotherm is characterized by a saturation zone [46]. Thus, the theoretical Langmuir isotherm is often used to describe the adsorption of a dissolved solution from a liquid solution as follows [47,48]:

$$Q_e = \frac{q_m K_L C_e}{1 + K_L C_e} \quad (3)$$

where $q_m$ and $K_L$ are the Langmuir constants, representing the maximum adsorption capacity, and the constant energy associated with the heat of adsorption. The two Langmuir constants can be

determined using the graphical representation ($C_e/Q_e$) function of ($C_e$) from the linear form of the Langmuir Equation:

$$\frac{C_e}{Q_e} = \frac{1}{(q_m \times K_L)} + \frac{C_e}{q_m} \quad (4)$$

Figure 5 shows the experimental data as well as the theoretical Langmuir model when the N-HAp nanopowder was used for the adsorption of $Pb^{2+}$ ions from aqueous solutions. The graphical representations of the $Pb^{2+}$ adsorbed ions on the mass unit by N-HAp powders, ($q_e$) depending on the concentration of $Pb^{2+}$ remaining in solution ($C_e$) are shown in Figure 5.

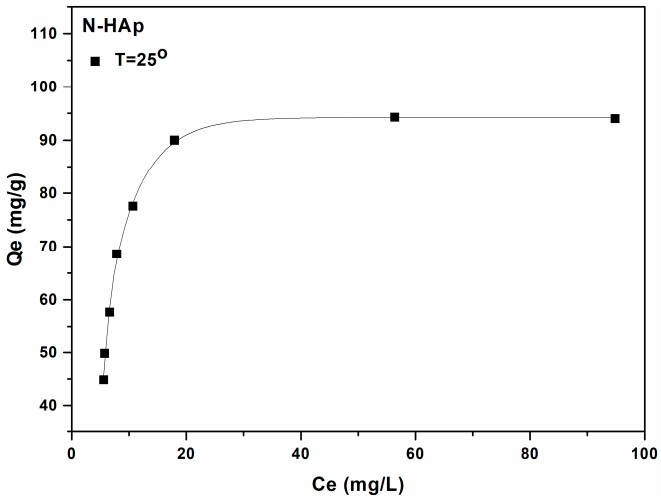


**Figure 5.** Graphic representation of the amount of material adsorbed at equilibrium by the equilibrium concentration for the adsorption of $Pb^{2+}$ ions on N-HAp powders.

Figure 5 shows the graphical representation of $C_e/Q_e$ function of $C_e$. The data has revealed that at ambient temperature, the $R^2$ coefficient deduced from the Langmuir isotherm is equal to 0.997 for N-HAp. In good agreement with previous studies [49,50], the transformation of the nonlinear isothermal equation into the linear form by a nonlinear method has not raised any problem. The two Langmuir constants were determined from the graphical representation of ($C_e/Q_e$) function of ($C_e$). Numerous studies have been reported in the literature on the ability of apatites and hydroxyapatite-based materials to adsorb metal ions from aqueous solutions. Depending on the experimental conditions of the adsorption process like pH solution, sorbent mass, initial concentration of pollutant material and the experiment duration, the adsorption capacity of $Pb^{2+}$ ions by hydroxyapatite was reported between 84 and 620 $mg \cdot g^{-1}$ [51]. Following the reaction of N-HAp with solutions contaminated with $Pb^{2+}$ ions, the lead ions were removed from the solutions and the hydroxyapatite dissolved. The Langmuir, $q_m$ and $K_L$ constants, representing the maximum adsorption capacity, and the constant energy associated with the heat of adsorption, were also determined using the graphical representation of the linear form of the Langmuir equation.

The results obtained from the adsorption batch experiments to remove lead ions from aqueous solutions using N-HAp powders have shown that N-HAp powders have been very effective in removing lead ions from the contaminated aqueous solutions. Thus, for the N-HAp samples an adsorption capacity of 99.31 mg (Pb)/g, and a $K_L$ coefficient value of 2.35 L/mg, was obtained. For a better understanding of the mechanisms involved in the removal of lead ions by N-HAp powders, the Freundlich model was also used. Freundlich adsorption isotherm [52] is the first known relationship that describes a non-ideal and reversible adsorption mechanism, which is not limited to monolayer formation. This empirical model can be applied in multilayer adsorption with uneven distribution of heat of adsorption and affinity of heterogeneous surfaces [53]. Historically, it was developed for the adsorption of animal-derived coal, demonstrating that the mass adsorbent ratio offered by the adsorbent and solutions is not constant at a different concentration of the solution [54]. From this

perspective, the adsorbed amount is the sum of the adsorption in all areas, with the stronger bonding zones being occupied first, and the adsorption energy decreases exponentially at the time of the adsorption process [55].

The Freundlich isotherm is described by the following Equation:

$$Q_e = k_f \times C_e^{\frac{1}{n}} \quad (5)$$

where $Q_e$ is the amount of material adsorbed at equilibrium (mg/g), $C_e$ is the metal ion concentration at equilibrium (mg/L) and $k_f$ [mg/g $(mg/L)^{-1/n}$] and n are Freundlich constants, representing the adsorption capacity and the adsorption intensity of the adsorbent.

The two Freundlich constants can be determined from the graphical representation ($lnQ_e$) function of ($lnC_e$) from the linear form of the Freundlich Equation:

$$lnQ_e = lnk_f + \frac{1}{n} lnC_e \quad (6)$$

Figure 6 shows the graphical representations of ($lnQ_e$) function of ($lnC_e$) for the lead ion adsorption experiments on N-HAp powders. The $k_f$, Freundlich constant, is an indicator of the adsorption capacity of the materials used as adsorbent, while 1/n is a function of the power adsorption from the process [56]. Figure 7 presents the Freundlich linearized fits for the adsorption of lead ions on N-HAp powders.

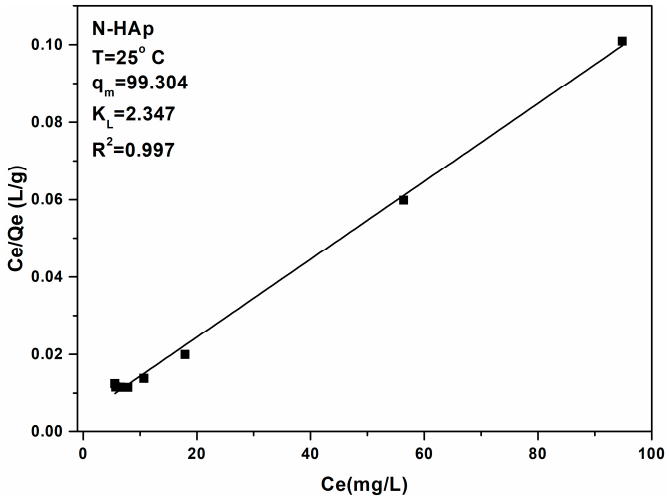


**Figure 6.** Langmuir linearized fits for the adsorption of lead ions on N-HAp.

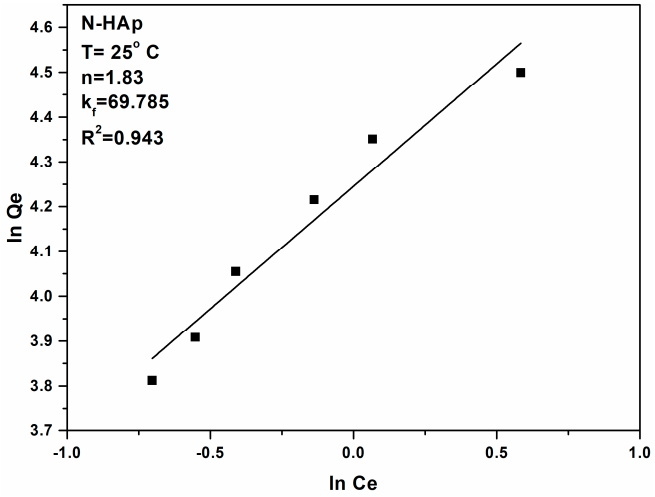


**Figure 7.** Freundlich linearized fits for the adsorption of lead ions on N-Hap.

If n = 1, then the separation of the two phases is independent of the concentration. If 1/n is below 1 this indicates a normal adsorption process. On the other hand, if 1/n is less than 1, this indicates a cooperative adsorption process [57]. According to the literature if the value of n is between one and ten, this indicates a favorable adsorption process [58]. The values obtained for n from the linearized form of the Freundlich equation (Figure 7), for the lead ion adsorption experiments on N-HAp powders were greater than 1 leading to a value of $1/n < 1$ thus signifying a normal adsorption process. Table 2 shows the values for both Langmuir and Freundlich constants obtained in the experiments to remove $Pb^{2+}$ ions from aqueous solutions using N-HAp powders.

**Table 2.** Langmuir and Freundlich isotherm parameters for $Pb^{2+}$ adsorption onto N-HAp nanopowders.

| Sample | Langmuir | | | Freundlich | | |
|---|---|---|---|---|---|---|
| N-HAp | $R^2$ | $q_m$ (mg/g) | $K_L$ (L/mg) | $R^2$ | n | $k_f$ |
| | 0.997 | 99.304 ± 0.2 | 2.347 ± 0.2 | 0.943 | 1.83 ± 0.3 | 69.785 ± 0.3 |

According with previous studies [59], the separation factor $R_L$ indicates the shape of isotherm, when $R_L > 1$, the isotherm is unfavorable, when $R_L = 1$, it is linear; when between 0 and 1, it is favorable and when $R_L = 0$ it is irreversible. In this study, the $R_L$ values were between 0 and 1 indicated a favorable adsorption of $Pb^{2+}$ on the adsorbent. It has also been observed that the uptake of Pb (II) throughout the process was high, due to the affinity that is relatively large between Pb (II) and N-HAp. Comparing the correlation coefficients ($R^2$), it can be deduced that the experimental equilibrium data of Pb (II) sorption was best suited to the Langmuir model. This behavior may be due to the homogeneous reaction on the surface for Pb (II) sorption. It was clearly seen that N-HAp was favorable for adsorption of Pb (II). The data obtained from adsorption isotherms of Pb (II) agreed with the Langmuir model. Furthermore, XRD analysis confirmed that the main mechanism in the adsorption of Pb (II) was due to the partial dissolution of N-HAp and pyromorphite reprecipitation. Similar results have been reported by Xu et al. [60], in their studies regarding lead immobilization by hydroxyapatite in aqueous solutions. The studies conducted by Xu et al. have revealed that the lead removal process using hydroxyapatite is kinetically fast. Moreover, they have emphasized that for a lead concentration of 100 $mg \cdot L^{-1}$ $Pb^{2+}$ the dominant reaction mechanisms involved in the adsorption process were the dissolution of hydroxyapatite and the precipitation of lead apatites such as hydroxypyromorphite in systems with no chloride, and of chloropyromorphite in systems that contain chloride [60]. The X-ray diffraction (XRD) patterns shown in Figure 8a evidenced the structural changes of N-HAp after Pb (II) adsorption. A mixed phase of pyromorphite ($Pb_{10}(PO_4)_6(OH)_2$) and HAp was revealed. In the TEM image was observed that the particles after sorption of lead have a more rounded shape (Figure 8b). More, from TEM image, it was observed that after the sorption of lead the particles increased their size and were crowded. The SEM image (Figure 8c) also showed agglomerated ellipsoidal particles in agreement with TEM image. The presence of lead in the recovered powder after the sorption of lead from the contaminated solution was also evidenced in the EDX spectrum (Figure 8d).

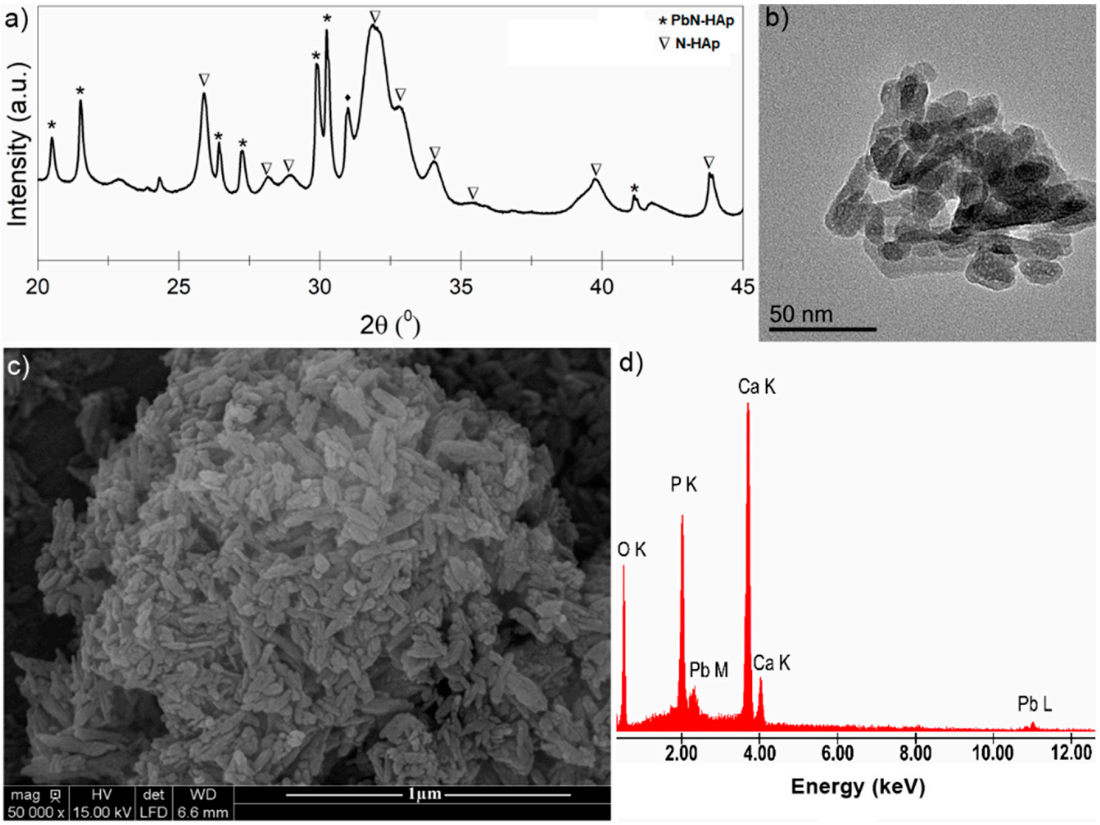


**Figure 8.** XRD patterns of N-HAp after lead immobilization (**a**); TEM image N-HAp after lead sorption (**b**); SEM image N-HAp after lead sorption (**c**); EDX spectra of N-HAp nanopowders (**d**).

Kinetic and equilibrium studies on the removal of Pb (II) from aqueous solution [61] have shown that the adsorption of lead cations (II) is due to the surface reaction with the hydroxyl terminal groups on the adsorbent and the combination of the positive charges of the metal cations with the negative charges on the adsorbent surfaces. The adsorption of Pb (II) ions by HAp can take place through various mechanisms. Functional groups, surface properties, structure are just a few factors that can affect the preference of adsorption. Moreover, the sorbate properties such as ionic size, molecular structure, ionic charge or concentration can also influence adsorption. On the other hand, the chemistry of tha solution such as the pH and ionic strength plays an important role in the adsorption mechanism. According to previous studies [19,20,62] it can be assumed that the adsorption properties of HAp nanopowders was mainly due to the functional groups $Ca^{2+}$, $PO_4{}^{3-}$, and $OH^-$ involved in the surface reactions. The previous studies [22,63,64] suggested that the first mechanism is the adsorption of Pb (II) ions on the HAp surfaces [22] that this mechanism is followed by ion exchange reaction between Pb (II) ions adsorbed and $Ca^{2+}$ ions of HAp [22].

Previous studies [22,65–68] confirmed that the main mechanism responsible for Pb (II) adsorption by HAp was the dissolution of HAp followed by precipitation of pyromphoritis (a more stable phase than HAp). According to these precedent studies [22,65–68], reactions could be described as follows:

The dissolution of HAp has been described as such:

$$Ca_{10}\ (PO_4)_6(OH)_2 + 14H^+ \rightarrow 10Ca^{2+} + 6HPO_4{}^- + 2H_2O \quad (7)$$

The pyromphoritis precipitation could be described as follows:

$$10Pb^{2+} + 6H_2PO_4{}^- + 2H_2O \rightarrow 4H^+ + Pb_{10}(PO_4)_6(OH)_2 \quad (8)$$

In agreement with the studies previously presented by Q.Y. Ma et al. [69] regarding the in situ lead immobilization by apatite, during dissolution/precipitation process there may be a proton exchange between the adsorbent and the metal ions in the solutions. So, the ≡POH site of HAp can transform into a ≡POPb$^+$ site.

Taking into account previous studies [70,71], we could say that adsorption of Pb (II) ions on the HAp surface which leads to replacement of Ca(II) could be attributed to the adsorption of Pb (II) by HAp and can be described as follows:

$$Ca_{10}(PO_4)_6(OH)_2 + xPb^{2+} \rightarrow Ca_{10-x}Pb_x(PO_4)_6 + xPb^{2+} \quad (9)$$

Z. Zhang et al. [72], in their studies on immobilization of lead and cadmium from aqueous solution and contaminated sediment using nano-hydroxyapatite, have shown that electronegativity and ionic radii in the range of 0.90–1.30 Å could be two other factors that influence the sorption capacity of HAp (ionic radius of $Ca^{2+}$ is 0.99 Å). The high sorption capacity obtained for lead could be explained by the high electronegativity of $Pb^{2+}$ (2.33) and the ionic radiation value of 1.20 Å. The results of this study were consistent with the the results presented by A. Corami et al. [73] in their studies on cadmium removal from single- and multi-metal (Cd + Pb + Zn + Cu) solutions by sorption on hydroxyapatite.

Our study is part of the overall effort to obtain effective adsorbents in the removal of heavy metal ions [74–76]. Hydroxyapatite being a non-toxic material has attracted attention due to its low cost and excellent adsorption properties for environmental applications. However, much effort has to be done to obtain materials that will increase the efficiency of removing heavy metal ions from aqueous systems as they pose a serious threat to public health and the ecological system due to high toxicity.

## 4. Conclusions

A nano hydroxyapatite was successfully synthesized and used for Pb (II) removal from aqueous solutions. The physico-chemical characterization of hydroxyapatite nanopowders obtained by an adapted coprecipitation method was explored. The obtained products presented a structure characteristic to the hexagonal hydroxyapatite and no additional peaks were found in the diffraction spectra of N-HAp. The morphology of N-HAp was nanometric size with ellipsoidal shaped particles. The efficiency of Pb (II) removal was analyzed by adsorption experiments. The removal efficiency of $Pb^{2+}$ ions was approximately 99.2% for lead concentrations in the range of 40–100 mg. The coefficient of regression ($R^2$) that was obtained using the Langmuir model was higher compared to that obtained using the Freundlich model. The results presented in this study could be useful for developing materials for environmental applications. Moreover, the material used as an adsorbent for removing heavy metals from contaminated waters is an ecological material that can be obtained at low costs.

**Author Contributions:** Conceptualization, D.P.; Methodology, D.P.; Validation, D.P., M.M.-H., S.L.I, R.G., M.B., and A.C.; Formal Analysis, D.P., M.M.-H., S.L.I., R.G., and A.C.; Investigation, D.P., and S.L.I.; Resources, D.P., M.M.-H., R.G., M.B., and S.L.I.; Data Curation, D.P. and S.L.I.; Writing—Original Draft Preparation, D.P.; Writing—Review & Editing, D.P., M.M-H., S.L.I., R.G., and A.C.; Visualization, D.P., M.M.-H., S.L.I, R.G., and A.C.; Supervision, M.M.-H. and R.G.; Project Administration, D.P.; Funding Acquisition, D.P.

**Funding:** This research was funded by a grant of the Romanian Ministry of Research and Innovation, UEFISCDI, through the projects "Improvement of Life Quality by Developing new Technologies Based on Efficient Nanoparticles in Water and Soil Decontamination-PN-III-P1-1.2-PCCDI-2017-0134", Contract Nr. 23PCCDI/2018, "Innovative Bionanomaterials for Treatment and Diagnosis PN-III-P1-1.2-PCCDI-2017-0629". Contract Nr. 43PCCDI/2018 and PICS 16BM/2016 and "The APC was funded by PN-III-P1-1.2-PCCDI-2017-0629, Contract Nr. 43PCCDI/2018".

**Acknowledgments:** We thank A. Richard and A. Sauldubois from the "Centre de Microscopie Electronique" of University of Orléans for assistance in SEM data acquisition. This work was (partially) supported by the following grants of the Romanian Ministry of Research and Innovation, PN-III-P1-1.2-PCCDI-2017-0134, PN-III-P1-1.2-PCCDI-2017-0629, Contract Nr. 43PCCDI/2018, Contract Nr. 23PCCDI/2018 and PICS 16BM/2016.

**Conflicts of Interest:** The authors declare no conflict of interest. The funders had no role in the design of the study; in the collection, analyses, or interpretation of data; in the writing of the manuscript, or in the decision to publish the results.

## References


1. Liao, D.; Zheng, W.; Li, X.; Yang, Q.; Yue, X.; Guo, L.; Zeng, G. Removal of lead(II) from aqueous solutions using carbonate hydroxyapatite extracted from eggshell waste. *J. Hazard. Mater.* **2010**, *177*, 126–130. [CrossRef] [PubMed]
2. Jang, S.H.; Min, B.G.; Jeong, Y.G.; Lyoo, W.S.; Lee, S.C. Removal of lead ions in aqueous solution by hydroxyapatite/polyurethane composite foams. *J. Hazard. Mater.* **2008**, *152*, 1285–1292. [CrossRef] [PubMed]
3. Raita, Ş.; Cornilă, N.; Danacu, V.; Rosu, P.; Barbuceanu, F. Histological researches concerning the pancreas in Struthio camelus Anatomia. Blackwell Verlag GmbH Ana. *Histol. Embryol.* **2014**, *43*, 74–75.
4. Iconaru, S.L.; Prodan, A.M.; Turculet, C.S.; Beuran, M.; Ghita, R.V.; Costescu, A.; Groza, A.; Chifiriuc, M.C.; Chapon, P.; Gaiaschi, S.; et al. Enamel Based Composite Layers Deposited on Titanium Substrate with Antifungal Activity. *J. Spectroscop.* **2016**, 4361051. [CrossRef]
5. Gillham, R.W.; O'Hannesin, R.S. Enhanced degradation of halogentaed aliphatics by zero-valent iron. *Ground Water* **1994**, *32*, 958–967. [CrossRef]
6. Biswas, P.; Wu, C.Y. Nanoparticles and the Environment, Critical Review Paper. *J. Air Waste Manag. Assoc.* **2005**, *55*, 708–746. [CrossRef] [PubMed]
7. Elliott, D.W.; Zhang, W.X. Field assessment of nanoscale bimetallic particles for groundwater treatment. *Environ. Sci. Technol.* **2000**, *35*, 4922–4926. [CrossRef]
8. Suciu, I.; Vârlan, C.; Dimitriu, B.; Soriţău, O.; Amza, O.; Moldoveanu, G.F.; Burlibaşa, M.; Gheorghe, I.; Lazar, V.; Gheorghiu, I. Biocompatibility Study of Several Esthetic Dental Restorative Materials. *Rom. Biotechnol. Lett.* **2016**, *21*, 11438–11442.
9. Predoi, D.; Predoi, M.V.; Iconaru, S.L.; Ech Cherif El Kettani, M.; Leduc, D.; Prodan, A.M. Ultrasonic Measurements on β Cyclodextrin/Hydroxyapatite Composites for Potential Water Depollution. *Materials* **2017**, *10*, 681. [CrossRef] [PubMed]
10. Raita, S.; Cornilă, N.; Dănacu, V.; Belu, C.; Georgescu, B.; Roşu, P.; Bărbuceanu, F. Morphological studies on the liver in Struthio camelus. Anatomia. Blackwell Verlag GmbH Ana. *Histol. Embryol.* **2014**, *43*, 74–75.
11. Prodan, A.M.; Beuran, M.; Turculet, C.S.; Popa, M.; Andronescu, E.; Bleotu, C.; Raita, S.M.; Soare, M.; Lupescu, O. In vitro evaluation of glycerol coated iron oxide nanoparticles in solution. *Rom. Biotechnol. Lett.* **2018**, *23*, 13901–13908.
12. Turculet, C.S.; Prodan, A.M.; Negoi, I.; Teleanu, G.; Popa, M.; Andronescu, E.; Beuran, M.; Stanciu, G.A.; Hristu, R.; Badea, M.L.; et al. Preliminary evaluation of the antifungal activity of samarium doped hydroxyapatite thin films. *Rom. Biotechnol. Lett.* **2018**, *23*, 13927–13932.
13. Zamani, S.; Salahi, E.; Mobasherpour, I. Removal of Nickel from aqueous solution by nano hydroxyapatite originated from Persian Gulf corals. *Can. Chem. Trans.* **2013**, *1*, 173–190.
14. Zhu, R.; Yu, R.; Yao, J.; Mao, D.; Xing, C.; Wang, D. Removal of $Cd^{2+}$ from aqueous solutions by hydroxyapatite. *Catal. Today* **2008**, *139*, 94–99. [CrossRef]
15. Milonjić, S.K. Comments on "factors influencing the removal of divalent cations by hydroxyapatite". *J. Hazard. Mater.* **2009**, *162*, 1588–1589. [CrossRef] [PubMed]
16. Iconaru, S.L.; Motelica-Heino, M.; Guegan, R.; Predoi, M.V.; Prodan, A.M.; Predoi, D. Removal of Zinc Ions Using Hydroxyapatite and Study of Ultrasound Behavior of Aqueous Media. *Materials* **2018**, *11*, 1350. [CrossRef] [PubMed]
17. Suzuki, T.; Hatsushika, T.; Hayakawa, Y. Synthetic hydroxyapatites employed as inorganic cation-exchangers. *J. Chem. Soc. Faraday Trans.* **1981**, *77*, 1059–1062. [CrossRef]
18. Gupta, S.S.; Bhattacharyya, K.G. Kinetics of adsorption of metal ions on inorganic materials: A review. *Adv. Colloid Inter. Sci.* **2011**, *162*, 39–58. [CrossRef] [PubMed]
19. Di Natale, F.; Erto, A.; Lancia, A.; Musmarra, D. A descriptive model for metallic ions adsorption from aqueous solutions onto activated carbons. *J. Hazard. Mater.* **2009**, *169*, 360–369. [CrossRef] [PubMed]
20. Erto, A.; Di Natale, F.; Musmarra, D.; Lancia, A. Modeling of single and competitive adsorption of cadmium and zinc onto activated carbon. *Adsorption* **2015**, *21*, 611–621. [CrossRef]
21. Suzuki, Y.; Takeuchi, Y. Uptake of a few divalent heavy metal ionic species by a fixed bed of hydroxyapatite particles. *J. Chem. Eng. Jpn.* **1994**, *27*, 571–576. [CrossRef]
22. Suzuki, T.; Ishigaki, K.; Miyake, M. Hydroxyapatites as inorganic cation exchangers. Part 3: Exchange characteristics of lead ions ($Pb^{2+}$). *J. Chem. Soc. Faraday Trans.* **1984**, *80*, 3157–3165. [CrossRef]

23. Martínez, C.E.; McBride, M.B. Aging of coprecipitated Cu in alumina: Changes in structural location, chemical form, and solubility. *Geochim. Cosmochim. Acta* **2000**, *64*, 1729–1736. [CrossRef]
24. Borum, L.; Wilson, O.C., Jr. Surface modification of hydroxyapatite. Part II. Silica. *Biomaterials* **2003**, *24*, 3681–3688. [CrossRef]
25. Ciobanu, C.S.; Constantin, L.V.; Predoi, D. Structural and physical properties of antibacterial Ag-doped nano-hydroxyapatite synthesized at 100 C. *Nanoscale Res. Lett.* **2011**, *6*, 613. [CrossRef] [PubMed]
26. Ciobanu, C.S.; Iconaru, S.L.; Le Coustumer, P.; Constantin, L.V.; Predoi, D. Antibacterial activity of silver-doped hydroxyapatite nanoparticles against gram-positive and gram-negative bacteria. *Nanoscale Res. Lett.* **2012**, *7*, 324. [CrossRef] [PubMed]
27. Ciobanu, C.S.; Iconaru, S.L.; Popa, C.L.; Motelica-Heino, M.; Predoi, D. Evaluation of samarium doped hydroxyapatite, ceramics for medical application: Antimicrobial activity. *J. Nanomater.* **2015**, *2015*, 849216. [CrossRef]
28. Ciobanu, C.S.; Andronescu, E.; Predoi, D. Bet and Xrd Studies on the Hydroxyapatite and Europium Doped Hydroxyapatite. *Dig. J. Nanomater. Biostruct.* **2011**, *6*, 1239–1244.
29. Ciobanu, C.S.; Iconaru, S.L.; Massuyeau, F.; Constantin, L.V.; Costescu, A.; Predoi, D. Synthesis, structure, and luminescent properties of europium-doped hydroxyapatite nanocrystalline powders. *J. Nanomater.* **2012**, 942801. [CrossRef]
30. Ciobanu, C.S.; Iconaru, S.L.; Le Coustumer, P.; Predoi, D. Vibrational Investigations of Silver-Doped Hydroxyapatite with Antibacterial Properties. *J. Spectrosc.* **2013**, 471061. [CrossRef]
31. Ciobanu, C.S.; Andronescu, E.; Stoicu, A.; Florea, O.; Le Coustumer, P.; Galaup, S.; Djouadi, A.; Mevellec, J.Y.; Musa, I.; Massuyeau, F.; et al. Influence of Annealing Treatment of Nano-Hydroxyapatite Bioceramics on the Vibrational Properties. *Dig. J. Nanomater. Biostruct.* **2011**, *6*, 609–624.
32. Ciobanu, C.S.; Iconaru, S.L.; Popa, C.L.; Costescu, A.; Motelica-Heino, M.; Predoi, D. Porous Methyltrimethoxysilane Coated Nanoscale-Hydroxyapatite for Removing Lead Ions from Aqueous Solutions. *J. Nanomater.* **2014**, 361061. [CrossRef]
33. Ślósarczyk, A.; Paszkiewicz, Z.; Paluszkiewicz, C. FTIR and XRD evaluation of carbonated hydroxyapatite powders synthesized by wet methods. *J. Mol. Struct.* **2005**, *744–747*, 657–661. [CrossRef]
34. Costescu, A.; Ciobanu, C.S.; Iconaru, S.L.; Ghita, R.V.; Chifiriuc, C.M.; Marutescu, L.G.; Predoi, D. Fabrication, Characterization, and Antimicrobial Activity, Evaluation of Low Silver Concentrations in Silver-Doped Hydroxyapatite Nanoparticles. *J. Nanomater.* **2013**, 194854. [CrossRef]
35. Cusco, I.R.; Guitian, F.; de Aza, S.; Arttis, L. Differentiation between Hydroxyapatite and β-Tricalcium Phosphate by Means of p-Raman Spectroscopy. *J. Eur. Ceram. Soc.* **1998**, *18*, 1301–1305. [CrossRef]
36. Brunauer, S.; Emet, P.H.; Teller, E. Adsorption of Gases in Multimolecular Layers. *J. Am. Chem. Soc.* **1938**, *60*, 309–319. [CrossRef]
37. Barrett, E.P.; Joyner, L.G.; Halenda, P.P. The determination of pore volume and area distributions in porous substances. I. Computations from nitrogen isotherms. *J. Am. Chem. Soc.* **1951**, *73*, 373–380. [CrossRef]
38. Cozmuta, L.M.; Cozmuta, A.M.; Peter, A.; Nicula, C.; Nsimba, E.B.; Tutu, H. The influence of pH on the adsorption of lead by Na-clinoptilolite: Kinetic and equilibrium studies. *Water SA* **2012**, *38*, 269–278. [CrossRef]
39. Zhang, M.; Jin, C.C.; Xu, L.H.; Ding, T. Effect of temperature, salinity, and pH on the adsorption of lead by sediment of a tidal river in east China. In Proceedings of the 2012 International Conference on Biomedical Engineering and Biotechnology, Macao, China, 28–30 May 2012.
40. Malek, A.; Farooq, S. Comparison of isotherm models for hydrocarbon adsorption on activated carbon. *AIChE J.* **1996**, *42*, 3191–3201. [CrossRef]
41. Langmuir, I. The constitution and fundamental properties of solids and liquids. *J. Am. Chem. Soc.* **1916**, *38*, 2221–2295. [CrossRef]
42. Bulut, E.; Ozacar, M.; Sengil, I.A. Adsorption of malachite green onto bentonite: Equilibrium and kinetic studies and process design. *Micropor. Mesopor. Mater.* **2008**, *115*, 234–246. [CrossRef]
43. Ncibi, M.C. Applicability of some statistical tools to predict optimum adsorption isotherm after linear and non-linear regression analysis. *J. Hazard. Mater.* **2008**, *153*, 207–212. [CrossRef] [PubMed]
44. Vijayaraghavan, K.; Padmesh, T.V.N.; Palanivelu, K.; Velan, M. Biosorption of nickel(II) ions onto Sargassum wightii: Application of two-parameterand three parameter isotherm models. *J. Hazard. Mater.* **2006**, *B133*, 304–308. [CrossRef] [PubMed]

45. Kundu, S.; Gupta, A.K. Arsenic adsorption onto iron oxide-coated cement (IOCC): Regression analysis of equilibrium data with several isotherm models and their optimization. *Chem. Eng. J.* **2006**, *122*, 93–106. [CrossRef]
46. Allen, S.J.; Mckay, G.; Porter, J.F. Adsorption isotherm models for basic dyea dsorption by peat in single and binary component systems. *J. Colloid Interface Sci.* **2004**, *280*, 322–333. [CrossRef] [PubMed]
47. Langmuir, I. The adsorption of gases on plane surfaces of glass, mica and platinum. *J. Am. Chem. Soc.* **1918**, *40*, 1361–1403. [CrossRef]
48. Ho, Y.S.; Huang, C.T.; Huang, H.W. Equilibrium sorption isotherm for metal ions on tree fern. *Process. Biochem.* **2002**, *37*, 1421–1430. [CrossRef]
49. Ho, Y.S. Selection of optimum sorption isotherm. *Carbon.* **2004**, *42*, 2115–2116. [CrossRef]
50. He, J.; Hong, S.; Zhang, L.; Gan, F.; Ho, Y.S. Equilibrium and Thermodynamic parameters of adsorption of merhylene blue onto rectorite. *Fresen. Environ. Bull.* **2010**, *19*, 2651–2656.
51. Minh, D.P.; Tran, N.D.; Nzihou, A.; Sharrock, P. Hydroxyapatite gel for the improved removal of $Pb^{2+}$ ions from aqueous. *Solution Chem. Eng. J.* **2013**, *232*, 128–138. [CrossRef]
52. Freundlich, H.M.F. Over the adsorption in solution. *J. Phys. Chem.* **1906**, *57*, 385–471.
53. Adamson, A.W.; Gast, A.P. *Physical Chemistry of Surfaces*, 6th ed.; Wiley-Interscience: New York, NY, USA, 1997.
54. Foo, K.Y.; Hameed, B.H. Insights into the modeling of adsorption isotherm systems. *Chem. Eng. J.* **2010**, *156*, 2–10. [CrossRef]
55. Zeldowitsch, J. Adsorption site energy distribution. *Acta Phys. Chim. URSS* **1934**, *1*, 961–973.
56. Voudrias, E.; Ytianos, F.; Bozani, E. Sorption Description isotherms of Dyes from aqueous solutions and Waste Waters with Different Sorbent materials, Global Nest. *Int. J.* **2002**, *4*, 75–83.
57. Mohan, S.; Karthikeyan, J. Removal of lignin and tannin color from aqueous solution by adsorption on to activated carbon solution by adsorption on to activated charcoal. *Environ. Pollut.* **1997**, *97*, 183–187. [CrossRef]
58. Goldberg, S. Equations and Models Describing Adsorption Processes in Soils. In *Chemical Processes in Soils*; Soil Science Society of America: Madison, WI, USA, 2005; p. 489.
59. Sangeetha, K.; Vidhya, G.; Vasugi, G.; Girija, E.K. Lead and cadmium removal from single and binary metal ion solution by novel hydroxyapatite/alginate/gelatin nanocomposites. *J. Environ. Chem. Eng.* **2018**, *6*, 1118–1126. [CrossRef]
60. Xu, Y.; Schwartz, F.W. Lead immobilization by hydroxyapatite in aqueous solutions. *J. Contam. Hydrol.* **1994**, *15*, 187–206. [CrossRef]
61. Mousavi, H.Z.; Seyedi, S.R. Kinetic and equilibrium studies on the removal of Pb (II) from aqueous solution using nettle ash. *J. Chil. Chem. Soc.* **2010**, *55*, 307–311. [CrossRef]
62. Zheng, W.; Li, X.; Yang, Q.; Zeng, G.; Shen, X.; Zhang, Y.; Liu, J. Adsorption of Cd(II) and Cu(II) from aqueous solution by carbonate hydroxylapatite derived from eggshell waste. *J. Hazard. Mater.* **2007**, *147*, 534–539. [CrossRef] [PubMed]
63. Zhan, X.M.; Zhao, X. Mechanism of lead adsorption from aqueous solutions using an adsorbent synthesized from natural condensed tannin. *Water Res.* **2003**, *37*, 3905–3912. [CrossRef]
64. Mousa, S.M.; Ammar, N.S.; Ibrahim, H.A. Removal of lead ions using hydroxyapatite nano-material prepared from phosphogypsum wast. *J. Saudi. Chem. Soc.* **2016**, *20*, 357–365. [CrossRef]
65. Hafsteinsdóttir, E.G.; Camenzuli, D.; Rocavert, A.L.; Walworth, J.; Gore, D.B. Chemical immobilization of metals and metalloids by phosphates. *Appl. Geochem.* **2015**, *59*, 47–62. [CrossRef]
66. Peng, Q.; Guo, J.; Zhan, Q.; Xiang, J.; Liu, B.; Zhou, A.; Liu, R.; Tian, Y. Unique Lead Adsorption Behavior of Activated Hydroxyl Group in Two-Dimensional Titanium Carbide. *J. Am. Chem. Soc.* **2014**, *136*, 4113–4116. [CrossRef] [PubMed]
67. Günay, A.; Arslankaya, A.; Tosun, I. Lead removal from aqueous solution by natural and pretreated clinoptilolite: Adsorption equilibrium and kinetics. *J. Hazard. Mater.* **2007**, *146*, 362–371. [CrossRef] [PubMed]
68. Vila, M.; Sandra Sánchez-Salcedo, S.; Vallet-Regí, M. Hydroxyapatite foams for the immobilization of heavy metals: From waters to the human body. *Inorg. Chim. Acta* **2012**, *393*, 24–35. [CrossRef]
69. Ma, Q.Y.; Traina, S.J.; Logan, T.J.; Ryan, J. In situ lead immobilization by apatite. *Environ. Sci. Technol.* **1993**, *27*, 1803–1810. [CrossRef]

70. Gandhi, M.R.; Meenakshi, G.N.K.S. Removal of copper(II) using chitin/chitosan nano-hydroxyapatite composite. *Int. J. Biol. Macromol.* **2011**, *48*, 119–124. [CrossRef] [PubMed]
71. Liang, W.; Zhan, L.; Piao, L.; Rüssel, C. Lead and copper removal fromaqueous solutions by porous glass derived calcium hydroxyapatite. *Mater. Sci. Eng. B* **2011**, *176*, 1010–1014. [CrossRef]
72. Zhang, Z.; Li, M.; Chen, W.; Zhu, S.; Liu, N.; Zhu, L. Immobilization of lead and cadmium from aqueous solution and contaminated sediment using nano-hydroxyapatite. *Environ. Pollut.* **2010**, *158*, 514–519. [CrossRef] [PubMed]
73. Corami, A.; Mignardi, S.; Ferrini, V. Cadmium removal from single- and multi-metal (Cd + Pb + Zn + Cu) solutions by sorption on hydroxyapatite. *J. Colloid Interface Sci.* **2008**, *317*, 402–408. [CrossRef] [PubMed]
74. Yang, Z.; Fang, Z.; Zheng, L.; Cheng, W.; Tsang, P.E.; Fang, J.; Zhao, D. Remediation of lead contaminated soil by biochar-supported nano-hydroxyapatite. *Ecotoxicol. Environ. Saf.* **2016**, *132*, 224–230. [CrossRef] [PubMed]
75. Yang, Z.; Fang, Z.; Tsang, P.E.; Fang, J.; Zhao, D. In situ remediation and phytotoxicity assessment of lead-contaminated soil by biochar-supported nHAP. *J. Environ. Manag.* **2016**, *182*, 247–251. [CrossRef] [PubMed]
76. Đorđević, M.P.; Maletaškić, J.; Stanković, N.; Babić, B.; Yoshidab, K.; Yano, T.; Matović, B. In-situ immobilization of Sr radioactive isotope using nanocrystalline hydroxyapatite. *Ceram. Int.* **2018**, *44*, 1771–1777. [CrossRef]